A molecular dynamics study of the influence of elongation and quadrupole moment upon some thermodynamic and transport properties of linear heteronuclear triatomic fluids

Ariel A. Chialvo, David L. Heath, and Pablo G. Debenedetti[a)]
Department of Chemical Engineering, Princeton University, Princeton, New Jersey 08544-5263

(Received 27 March 1989; accepted 7 September 1989)

The influence of elongation, quadrupole strength, temperature, and number density upon the pressure, energy, translational diffusion, rotational relaxation, and shear viscosity of linear, rigid, three-site, heteronuclear, shifted-force Lennard-Jonesiums (RTSLJ) was studied via (N,V,T) molecular dynamics. For quadrupolar systems, molecular elongation was systematically perturbed about a base case, with quadrupole strengths scaling as the square of the elongation. The same elongation perturbations were applied to otherwise identical, nonquadrupolar systems. At constant density, the configurational energy increases in magnitude with elongation for the quadrupolar systems, and decreases in the nonquadrupolar case. The pressure exhibits a maximum at intermediate elongation in the presence of quadrupolar interactions, and increases monotonically with elongation at constant density for nonquadrupolar systems. Center-of-mass mobility decreases due to the presence of quadrupolar interactions, which also tend to slow down rotational relaxation rates.

INTRODUCTION

The quantitative prediction of fluid properties from knowledge of the molecular architecture of the constituent species remains a challenging problem. Molecular dynamics (MD) is a valuable tool for the investigation of both equilibrium and time-dependent behavior in model fluids. It is a distinguishing feature of this method that it provides essentially exact answers to idealized problems. The nature of the idealization lies in the representation of molecular architecture and intermolecular potentials; the latter, in particular, are, at best, plausible approximations to physical reality. The usefulness of MD, therefore, it not as a predictive technique. Rather, it allows the rigorous testing of theories (when they exist), it provides exact results on well-defined models which might stimulate the development of theories, and, more importantly in the present context, it enables the systematic investigation of the relationship between bulk properties and molecular architecture in model systems.

In nature, chemical species differ from each other in a great variety of ways, which include mass, mass distribution, shape, electrical charge distribution, bond angles and flexibility, etc. Bulk behavior, therefore, is the result of the complicated interaction among the above factors. A fundamental understanding of complex phenomena is usually based upon a clear knowledge of simplified, idealized problems, in which the underlying causes act separately. This can be done most effectively in molecular-based simulations, where the architecture and interaction laws which define the model under study can be selectively perturbed, and the results of such perturbations measured exactly. Such is the approach underlying the present work.

Recent examples of the application of MD to investigate the relationship between transport in dense fluids and the underlying details of molecular architecture include the work of Brown and Clarke,[1] who studied the effect of mass distribution on mass and momentum transport in rigid nonlinear triatomic molecules, and that of Hoheisel,[2] who compared the translational diffusivities of planar (benzene-like) and "globular" (SF_6-like) model systems. Here, we focus our attention on triatomic molecular fluids composed of linear molecules with a net quadrupole moment. The model used in this work is a rigid, three-site heteronuclear Lennard-Jonesium with point quadrupole (RTSLJQ), a plausible idealization of CO_2. Carbon dioxide differs from other linear molecular fluids in that it possesses a very large quadrupole (more than three times greater than that of N_2 [3]). Electrostatic interactions play a correspondingly more important role in both the equilibrium and time-dependent properties of solid and dense fluid CO_2 than they do in, say, N_2.[4]

Previous work on the time-dependent behavior of linear model systems in the spirit of this investigation (i.e., systematic perturbations of molecular elongation and/or quadrupole moment) has focused on homonuclear diatomic fluids, and includes the work of Steele and Streett[5] on translational and rotational motion in quadrupolar diatomics, and that of Singer *et al.*[6] on the translational and rotational autocorrelation functions of two-site Lennard-Jonesiums. Kabadi and Steele[7] have studied the temperature dependence of rotational and translational dynamics of quadrupolar diatomic Lennard-Jonesiums, at a fixed value of density and elongation. Several aspects of the equilibrium behavior of Lennard-Jonesiums with quadrupolar interactions have been studied via computer simulations.[8–11] The work of English and Venables,[12] on the other hand, is an important example of the use of systematic perturbations in elongation and quadrupole strength as a method for the investigation of solid state properties. These authors studied the effects of said variables upon the stability of crystal structures of homonuclear diatomic molecular solids modeled via two-center Lennard-Jonesiums with point quadrupolar interactions.

In their important study of homonuclear Cl_2 and Br_2-

a) To whom correspondence should be addressed.

 0021-9606/89/247818-13$02.10

like diatomics, Steele and Streett[5] studied four different systems: a purely repulsive diatomic in which the Lennard-Jones potential was shifted by a value equal to the well depth and truncated past a separation corresponding to the location of the well depth, a nonquadrupolar diatomic, and two different quadrupolar diatomics in which the reduced quadrupole moment was varied by a factor of $\sqrt{2}$. These authors investigated both thermodynamic (energy, pressure) and time-dependent (translational and rotational motion) behavior. They considered only perturbations in the quadrupole at fixed elongation, and at a single state point. Density, temperature, and elongation effects were not considered.

In this paper, we investigate the effects of quadrupole moment, elongation, number density, and temperature upon equilibrium (pressure, energy) and time-dependent (rotational and translational diffusion, shear viscosity) properties of linear heteronuclear triatomic fluids.

SYSTEMS AND STATE CONDITIONS

The systems studied in this work are described in Table I. The notation *s, m, l,* denotes short, medium, and long molecule; *QQ* and no *QQ* refer to the presence or absence of quadrupolar interactions, respectively. Rigid, three-site, linear, heteronuclear Lennard-Jonesiums were considered in all cases, with a carbon-like site at the center and two symmetric oxygen-like sites at the extremes. Size and energy parameters for the site–site interactions are identical to those used by Murthy *et al.*[4] (model C), in their study of interaction site models for carbon dioxide. The intermediate elongation (m) is also identical to that used by Murthy *et al.*[4] (model C). Molecular elongations were perturbed by a factor of $\sqrt{2}$ about the intermediate value, with simulations therefore spanning a factor of 2 in this variable.

Electrostatic interactions were modeled via a point quadrupole potential[13] (see Appendix for technical details pertaining to all simulations). The reduced quadrupole strength Q^* used with the medium elongation (m), corresponds to a quadrupole moment of -1.284×10^{-39} C m^2, again identical to that used by Murthy *et al.*[4] Thus, the medium molecule has an oxygen–oxygen separation of 2.32 Å (the gas-phase value[4] for CO_2), and a quadrupole moment which is 89% of the measured value[3] for CO_2. Quadrupole strengths were perturbed by a factor of 2 in each direction about the intermediate value (m): this corresponds to a change in elongation by a factor of $\sqrt{2}$ (see above) at constant effective charges at the oxygen-like sites. Consequently, the oxygen–oxygen separation for the long molecule is 41.4% greater than in gaseous CO_2, and its quadrupole moment, 79% higher.

State conditions investigated in this work are sumarized in Table II. The intermediate density is very close to CO_2's critical density ($\rho_c^* = 0.1384$)[14]; simulations span a factor of 10 in density. The high density corresponds to liquid CO_2 at its triple point. The low temperature is 3.4 K higher than CO_2's triple point, while the high temperature is 30 K above its critical point. All simulations were performed in the (N,V,T) ensemble (see Appendix for technical details). In this work, we use a reduced density based on σ_{CC}^3 (neither σ_{CC} nor σ_{OO} were perturbed during the simulations). A nondimensionalization based on the molecular volume[15] would result instead in an elongation-dependent volume fraction. Since we are interested in investigating the effects of given elongation perturbations at constant number density, the former approach (i.e., scaling density with a Lennard-Jones σ) was adopted, as in the work of Kabadi and Steele.[7]

As discussed in the Introduction, our goal is to understand the influence of geometry and charge distribution upon the properties of linear heteronuclear triatomic fluids and not to model the behavior of CO_2 by fitting intermolecular potential parameters. Nevertheless, in the Appendix, we compare calculated properties for the CO_2-like system (m,QQ) with experimental results for CO_2.

THERMODYNAMIC PROPERTIES

Table III lists the calculated pressure, configurational energy, translational diffusion coefficients, and shear viscosities, together with the corresponding systems and state conditions, as per Tables I and II. All systems exhibited fluid behavior: no plateaus in mean squared displacement were detected. In the case of the long molecule with quadrupolar interactions at low temperature (l,QQ,$T^* = 7.586$), the reduced mobility suggests proximity to a freezing transition. Even in this case, though, the diffusion coefficient is several orders of magnitude higher than solid-phase diffusivities.

The density and elongation dependence of the configurational energy is shown in Figs. 1 and 2, where the tempera-

TABLE I. Summary of systems investigated in this work.

System	l^* (d_{OO}/σ_{CC})	$Q^{*\,a}$ $Q'/(\sigma_{CC}^5\epsilon_{CC})^{1/2\,b}$
s, no QQ	0.589	0
m, no QQ	0.833	0
l, no QQ	1.178	0
s, QQ	0.589	−2.35
m, QQ	0.833	−4.70
l, QQ	1.178	−9.40

Site–site LJ potential parameters

$\sigma_{CC} = 2.785$ Å	$\sigma_{OO} = 3.014$ Å	$2\sigma_{CO} = (\sigma_{OO} + \sigma_{CC})$
$\epsilon_{CC}/k = 29$ K	$\epsilon_{OO}/k = 83.1$ K	$\epsilon_{CO} = (\epsilon_{OO}\epsilon_{CC})^{1/2}$

[a] $Q(\text{C m}^2) = 2.732\times10^{-40}Q^*$.
[b] $Q' = Q(4\pi\epsilon_0)^{-1/2}$; $\epsilon_0 = 8.8542\times10^{-12}$ C^2 N^{-1} m^{-2}.

TABLE II. State conditions investigated in this work.

ρ^{*a} $(\rho\sigma_{CC}^3)$	$T^{*\,b}$ (kT/ϵ_{CC})
0.0347	11.517
0.1381	11.517
0.348	11.517
0.348	7.586

[a] ρ (mol/m^3) $= 7.69\times10^4\rho^*$.
[b] $T(K) = 29T^*$.

TABLE III. Calculated thermodynamic and transport properties.[a]

ρ^* ($\rho\sigma_{cc}^3$)	T^* (kT/ϵ_{cc})	System	U^*[b] ($U/N\epsilon_{cc}$)	P^*[c] ($P\sigma_{cc}^3/\epsilon_{cc}$)	D_t^*[d] $[D_t\sqrt{m_{CO_2}}/(\sigma_{cc}\sqrt{\epsilon_{cc}})]$	η^*[e] $[\eta\sigma_{cc}^2/\sqrt{m_{CO_2}\epsilon_{cc}}]$
0.0347	11.517	*s*, no *QQ*	-4.46 ± 0.01	0.343 ± 0.005	12.25	1.9
0.0347	11.517	*m*, no *QQ*	-3.70 ± 0.01	0.367 ± 0.005	11.29	1.7
0.0347	11.517	*l*, no *QQ*	-3.14 ± 0.01	0.402 ± 0.006	9.21	2.5
0.0347	11.517	*s*, *QQ*	-4.48 ± 0.01	0.339 ± 0.005	10.83	0.9
0.0347	11.517	*m*, *QQ*	-4.73 ± 0.01	0.352 ± 0.005	9.89	1.0
0.0347	11.517	*l*, *QQ*	-76.1 ± 0.1	0.050 ± 0.001	3.25	0.7
0.1381	11.517	*s*, no *QQ*	-15.64 ± 0.02	0.96 ± 0.01	2.79	3.5
0.1381	11.517	*m*, no *QQ*	-13.42 ± 0.02	1.38 ± 0.02	2.54	4.3
0.1381	11.517	*l*, no *QQ*	-12.19 ± 0.02	2.15 ± 0.03	1.83	4.0
0.1381	11.517	*s*, *QQ*	-16.50 ± 0.02	0.89 ± 0.01	2.55	1.9
0.1381	11.517	*m*, *QQ*	-17.51 ± 0.03	1.14 ± 0.01	2.43	1.6
0.1381	11.517	*l*, *QQ*	-97.0 ± 0.1	-0.260 ± 0.004	0.44	1.6
0.348	11.517	*s*, no *QQ*	-37.26 ± 0.06	5.74 ± 0.08	0.89	9.3
0.348	11.517	*m*, no *QQ*	-33.87 ± 0.05	16.9 ± 0.2	0.51	9.9
0.348	11.517	*l*, no *QQ*	-27.40 ± 0.04	40.1 ± 0.5	0.37	8.3
0.348	11.517	*s*, *QQ*	-37.91 ± 0.06	5.66 ± 0.08	0.62	3.4
0.348	11.517	*m*, *QQ*	-43.60 ± 0.06	13.0 ± 0.2	0.39	4.6
0.348	11.517	*l*, *QQ*	-128.2 ± 0.2	3.73 ± 0.05	0.07	4.1
0.348	7.586	*s*, no *QQ*	-40.00 ± 0.06	-0.88 ± 0.01	0.55	...
0.348	7.586	*m*, no *QQ*	-37.40 ± 0.05	7.3 ± 0.1	0.33	...
0.348	7.586	*l*, no *QQ*	-33.10 ± 0.05	26.3 ± 0.4	0.22	...
0.348	7.586	*s*, *QQ*	-41.05 ± 0.06	-0.98 ± 0.01	0.41	...
0.348	7.586	*m*, *QQ*	-49.64 ± 0.07	2.77 ± 0.04	0.19	...
0.348	7.586	*l*, *QQ*	-144.1 ± 0.2	-5.80 ± 0.08	0.01	...

[a] See Table IV for rotational motion.
[b] $U(\text{J/mol}) = 241.12\,U^*$.
[c] $P(\text{bar}) = 185.42\,P^*$.
[d] $D_t\ (\text{cm}^2/\text{s}) = 2.0616\times10^{-4}\,D_t^*$; estimated accuracy (see the Appendix): $\pm 6\%$.
[e] $\eta\ (\text{cp}) = 6.976\times10^{-2}\,\eta^*$: estimated accuracy (see the Appendix): $\pm 13\%$.

ture was kept at $T^* = 11.517$. We note (Fig. 1) that the magnitude of the configurational energy increases in almost linear fashion with density for a given elongation and quadrupole moment.

Note that the quadrupolar energy is quadratic in quadrupole strength and hence, in this study, quartic in elongation. Hence the high negative U^* values reported in Table III for the (l,QQ) case. The ratio $U(l,\text{QQ})/U(s,\text{QQ})$ is 17 at

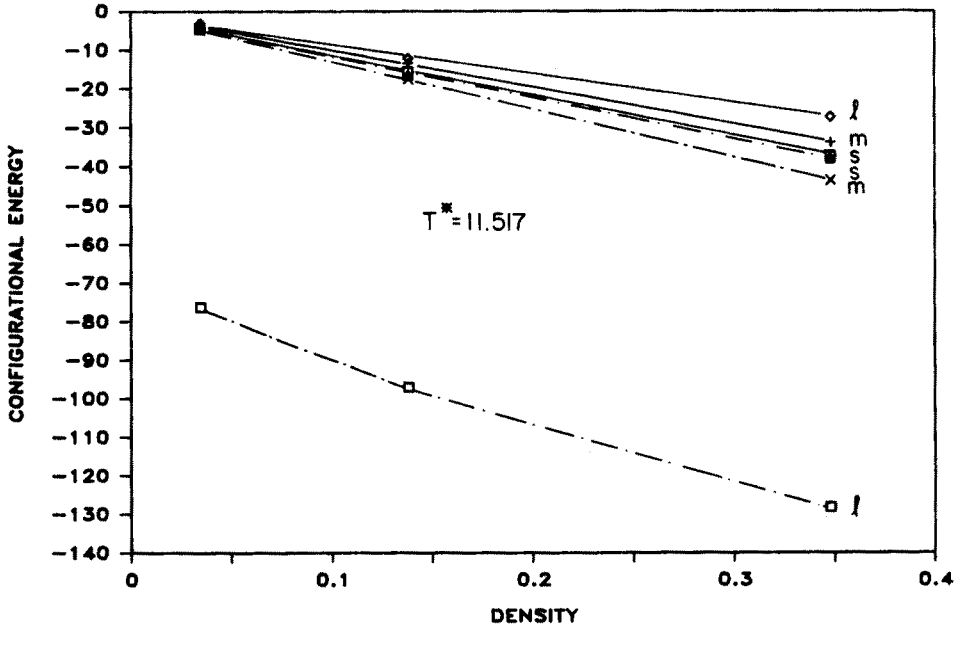

FIG. 1. Dependence of the configurational energy per molecule (U^*) upon density (ρ^*) for nonquadrupolar (—) and quadrupolar (–·–) systems. $T^* = 11.517$, *s*, *m*, and *l* denote the small, medium, and long molecule, respectively.

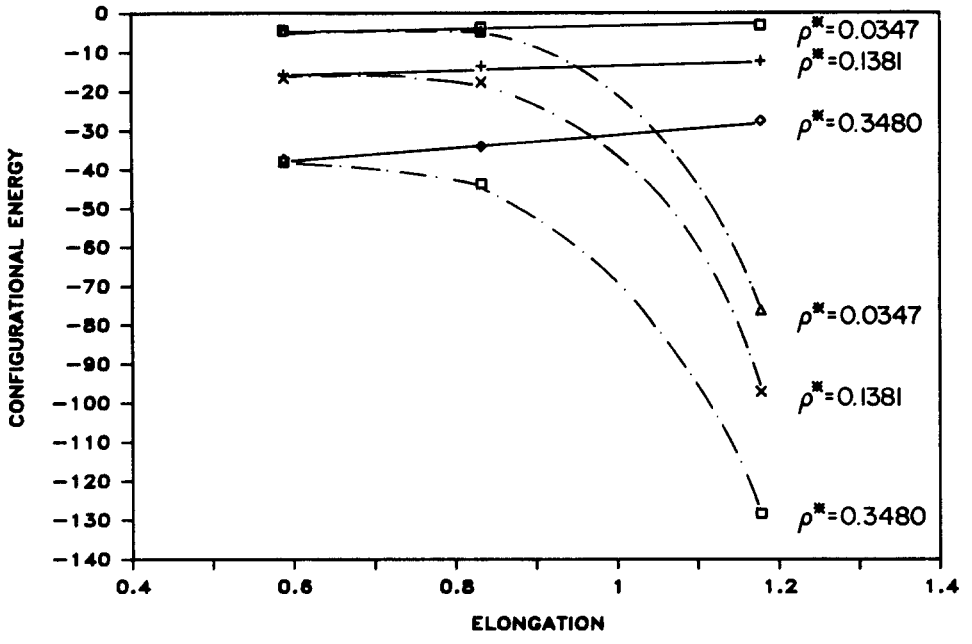

FIG. 2. Dependence of the configurational energy per molecule (U^*) upon molecular elongation (d_{OO}/σ_{CC}) for nonquadrupolar (—) and quadrupolar(–·–) systems. $T^* = 11.517$.

low density, and smaller thereafter. The corresponding ratio of fourth powers of elongations is 16.

It can be seen from Fig. 2 that the presence of quadrupolar interactions gives rise to behavior which differs from its quadrupole-free counterpart in qualitative as well as quantitative ways. Thus, whereas the magnitude of the configurational energy decreases linearly with elongation at constant density in the absence of quadrupolar interactions, the same quantity grows in nonlinear fashion as the elongation is increased at constant density in the presence of quadrupolar interactions. This important thermodynamic feature cannot be obtained by adjusting the values of the site Lennard-Jones parameters, and would be lost completely in the absence of quadrupolar interactions.

Figure 3 shows the density dependence of the pressure, with elongation and quadrupole moment as parameters, at $T^* = 11.517$. The pressure increases with elongation at constant density in the absence of quadrupole–quadrupole interactions, but decreases upon addition of a quadrupole moment at constant density and elongation (Table III), the latter trend having been previously reported by Steele and Streett[5] in their study of homonuclear, quadrupolar diatomics. The pressure extremun at intermediate elongation for quadrupolar systems at low, medium, and high density (Table III) is therefore the result of these opposing effects.

Differences between the thermodynamic behavior of linear molecular fluids with and without quadrupolar interactions, therefore, are not merely quantitative, but qualitative. The magnitude of the configurational energy decreases with elongation at constant density for a nonquadrupolar

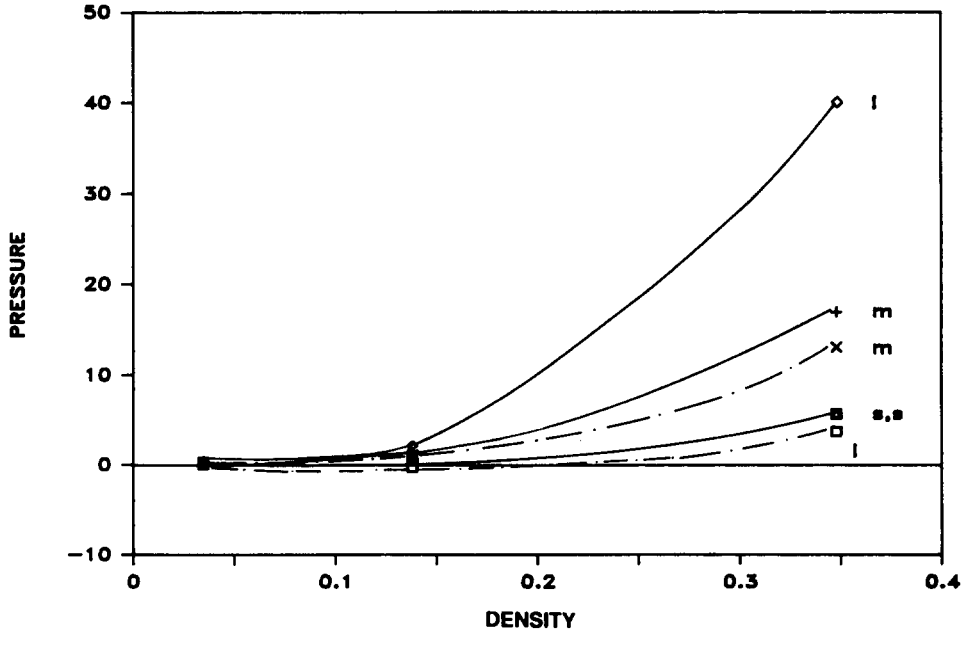

FIG. 3. Dependence of pressure (P^*) upon density (ρ^*) for nonquadrupolar (—) and quadrupolar (–·–) systems. $T^* = 11.517$. *s*, *m*, and *l* denote the small, medium, and long molecule, respectively.

system, but increases with elongation for a quadrupolar system. Similarly, at constant density, the pressure increases with elongation in a nonquadrupolar system, but exhibits a maximum at intermediate elongation in the quadrupolar case.

TIME-DEPENDENT BEHAVIOR

Translational motion

Table III includes the calculated diffusion coefficients, together with the corresponding systems and state conditions, as per Tables I and II. Diffusivities were computed from time-and-ensemble-averaged mean squared center-of-mass displacement vs time curves (see Appendix for technical details). The data corresponding to $T^* = 11.517$ are plotted in Fig. 4, with elongation as independent variable and density and quadrupole as parameters.

In the absence of quadrupolar interactions, the ratio of diffusion coefficients of the medium molecule to those of the long molecule equals 1.38 ($\rho^* = 0.348$), 1.39 ($\rho^* = 0.1381$), and 1.23 ($\rho^* = 0.0347$), while the length ratio (l/m) is 1.414. The approximate agreement between ratios of diffusivities and length at high and intermediate densities is indicative of hydrodynamic (Stokes–Einstein) behavior, with the "hydrodynamic size" of the molecules scaling as their only characteristic dimension (i.e., their length). The corresponding ratios for the short and medium molecules (s/m) are 1.75 ($\rho^* = 0.348$), 1.1 ($\rho^* = 0.1381$), and 1.09 ($\rho^* = 0.0347$). Thus, we see breakdown of hydrodynamic behavior even at liquid-like densities for the short molecule. Analogous calculations for the case of quadrupolar interactions are meaningless in this study, since elongation and quadrupole moment are not independent.

Quadrupolar attractions tend to decrease translational mobility (Table III, Fig. 4). This agrees with the observations of Steele and Streett[5] for diatomic Lennard-Jonesiums at fixed elongation, temperature, and density. The present study shows that this effect becomes more pronounced at high density and elongation, as can be seen from calculating the ratios of nonquadrupolar to quadrupolar diffusivities for the short, medium, and long molecules.

Density effects are summarized in Fig. 5, where the data of Fig. 4 has been replotted, with elongation (and quadrupole) as parameters, and density as independent variable. Upon increasing the bulk density, there is a pronounced decrease in the overall range of diffusivities spanned as a result of changes in elongation and quadrupolar strength [i.e., $D(s,$ no QQ$) - D(l,$QQ$)$]. Note, however, that the corresponding ratio [i.e., $D(s,$ no QQ$)/D(l,$QQ$)$] actually increases, from 3.77 ($\rho^* = 0.0347$) to 12.71 ($\rho^* = 0.348$).

Rotational motion

Rotational motion can be conveniently analyzed within the framework of Debye's theory of angular relaxation.[16] In this approach, one assumes the existence of a time Δt large enough so that successive angular displacements are uncorrelated, yet small enough so that, during this interval, only small displacements occur.[16] This being so, one can write a diffusion equation for the probability distribution function of molecular orientations f[16–18]. This quantity is defined in such a way that the differential probability $d\omega$ of finding a molecule with an orientation within $d\theta$ of θ, and within $d\phi$ of ϕ, is given by $d\omega = f\, d\phi \sin\theta\, d\theta$, where (θ,ϕ) are the polar and azimuthal angles of a molecule's orientation vector with respect to a laboratory frame. Since we are interested in displacements with respect to an initial orientation, and not with respect to a laboratory frame, we seek a solution to the diffusion equation for f, subject to the initial condition $2\pi f(\theta,\phi,0) = \delta(\cos\theta - 1)$, where now

$$\cos\theta(t) = \mathbf{l}(t)\cdot\mathbf{l}(0) \qquad (1)$$

with $\mathbf{l}$, the unit vector coaxial with the linear molecule. The

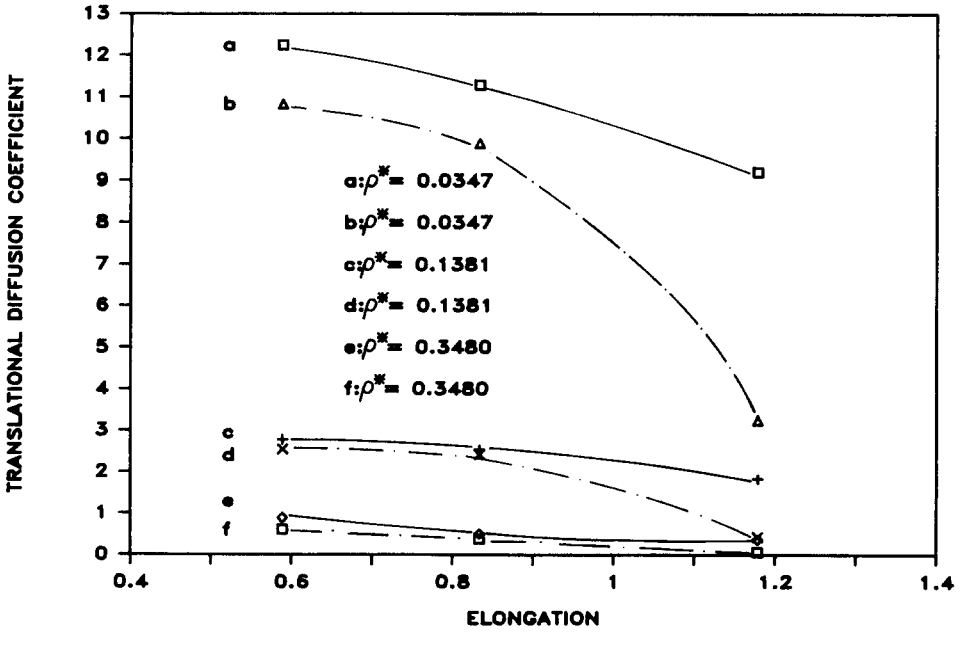

FIG. 4. Dependence of translational diffusion coefficients (D_T^*) upon molecular elongation (d_{OO}/σ_{CC}) for nonquadrupolar (—) and quadrupolar (–·–) systems. $T^* = 11.517$.

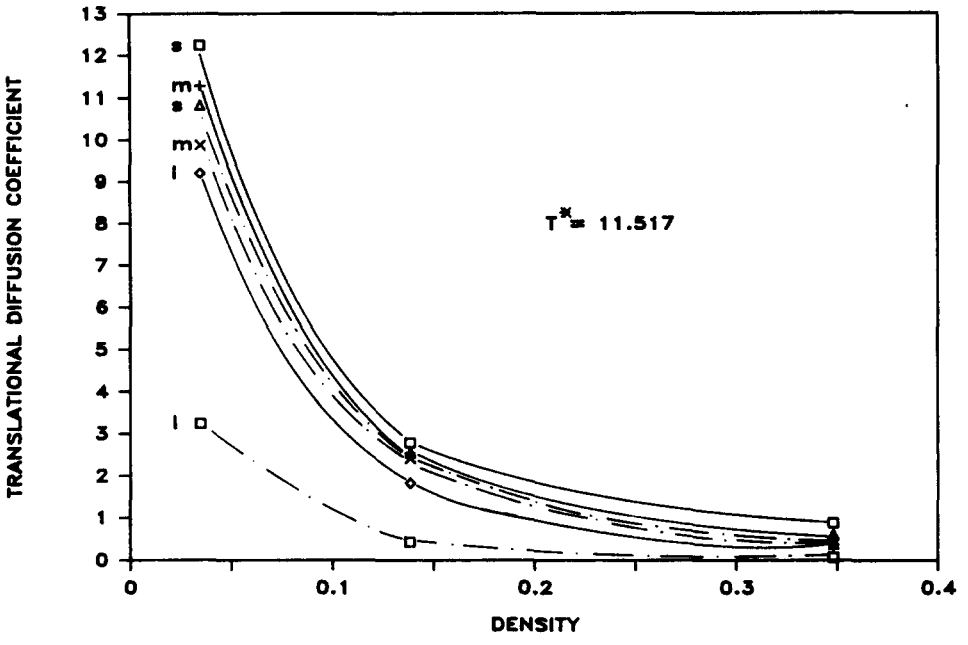

FIG. 5. Dependence of translational diffusion coefficients (D_t^*) upon density (ρ^*) for nonquadrupolar (—) and quadrupolar (–·–) systems. $T^* = 11.517$. *s*, *m*, and *l* denote the small, medium, and long molecule, respectively.

solution to the diffusion equation subject to the pulse initial condition reads[17,18]

$$f(\theta,t) = \sum_{j=0}^{\infty} \left(\frac{2j+1}{4\pi}\right) P_j[\cos\theta(t)] \exp\{-j[(j+1)]D_R t\}, \tag{2}$$

where $P_j(x)$ is the jth order Legendre polynomial [$P_0(x) = 1$; $P_1(x) = x$; $P_2(x) = 1.5x^2 - 0.5$], and D_R is the rotational diffusion coefficient. Equation (2) and the normalization condition $\int d\omega = 1$ imply

$$\langle \cos\theta(t) \rangle = \exp(-2D_R t), \tag{3}$$

$$\langle 1.5\cos^2\theta(t) - 0.5 \rangle = \exp(-6D_R t). \tag{4}$$

In addition, for $t \gg (10D_R)^{-1}$, we can neglect all but the leading terms in the expression for $f(\theta,t)$[17] [i.e., Eq. (2)], and we can write

$$\langle \theta^2(t) \rangle \cong \frac{\pi^2 - 4}{2} - \frac{3\pi^2}{8}\exp(-2D_R t) + \frac{10}{9}\exp(-6D_R t), \tag{5}$$

where

$$\langle A(\theta,\phi,t) \rangle \equiv \int_0^{2\pi} d\phi \int_0^{\pi} d\theta \sin\theta f(\theta,\phi,t) A(\theta,\phi,t). \tag{6}$$

According to the Debye theory, then, $\langle P_1(\cos\theta) \rangle$ and $\langle P_2(\cos\theta) \rangle$ decay exponentially, with relaxation times τ_1 and τ_2 satisfying

$$\tau_1 = (2D_R)^{-1} \tag{7}$$

$$\tau_2 = (6D_R)^{-1}. \tag{8}$$

Since the physical picture upon which the theory is based is that of noninteracting particles undergoing small and random (Brownian) rotations between collisions,[18] it is not *a priori* evident that the systems under study here obey Eq. (3) or (4), especially at low density. Thus, we are interested in investigating the effects of density, quadrupolar interactions, and elongation upon the validity of the Debye theory for the quantification of rotational motion in molecular fluids composed of small linear molecules, such as carbon dioxide.

Calculated rotational relaxation times and diffusion coefficients are listed in Table IV. Relaxation times were obtained from the condition

$$\ln\langle P_j[\cos\theta(\tau_j)] \rangle = -1 \quad (j = 1,2). \tag{9}$$

Note that Eq. (9) is an objective measure of rotational relaxation, irrespective of whether the decay of the first two Legendre polynomials is indeed exponential (as demanded by Debye's theory) or not. If the hypotheses underlying Debye's theory are valid, one must have $\tau_1/\tau_2 = 3$, and the relaxation times are true properties of the system. If the decay of the Legendre polynomials is not exponential, on the other hand, τ_1 and τ_2 are qualitative indicators of rotational relaxation but are not, strictly speaking, properties. Rotational diffusion coefficients were obtained from the decay of the Legendre polynomials

$$D_{R1} = \frac{1}{2}\frac{d}{dt}\{-\ln\langle P_1[\cos\theta(t)] \rangle\}, \tag{10}$$

$$D_{R2} = \frac{1}{6}\frac{d}{dt}\{-\ln\langle P_2[\cos\theta(t)] \rangle\}. \tag{11}$$

If the hypotheses underlying Debye's theory are valid, one must have linear behavior and $D_{R1} = D_{R2} = D_R$. Ensemble averages in Eqs. (9)–(11) were computed by averaging over all molecules, and over initial times (see Appendix for details).

In calculating rotational diffusion coefficients via Eqs. (10) and (11), care must be exercised to allow the system to relax beyond the initial regime during which the Legendre polynomials decay nonexponentially.[5,19] For homonuclear, quadrupolar, Lennard-Jones diatomics, this initial relaxation time is of the order of 0.3 ps[5] (or 0.08 dimensionless time units; see Table IV). At long times, on the other hand, the

TABLE IV. Calculated rotational relaxation times and diffusion coefficients.

ρ^* ($\rho\sigma_{CC}^3$)	T^* (kT/ϵ_{CC})	System	τ_1^{*} [a,b] $\left[\frac{\tau_1\sqrt{\epsilon_{CC}}}{(\sigma_{CC}\sqrt{m_{CO_2}})}\right]$	τ_2^{*} [a,b] $\left[\frac{\tau_2\sqrt{\epsilon_{CC}}}{(\sigma_{CC}\sqrt{m_{CO_2}})}\right]$	τ_1^*/τ_2^*	D_{R1}^{*} [c,d,e] $\left[\frac{D_{R1}\sigma_{CC}\sqrt{m_{CO_2}}}{\sqrt{\epsilon_{CC}}}\right]$	D_{R2}^{*} [c,d,e] $\left[\frac{D_{R2}\sigma_{CC}\sqrt{m_{CO_2}}}{\sqrt{\epsilon_{CC}}}\right]$	D_{R1}^*/D_{R2}^*
0.0347	11.517	*s*, no *QQ*	0.069	0.042	1.643	···	···	···
0.0347	11.517	*m*, no *QQ*	0.099	0.059	1.678	···	···	···
0.0347	11.517	*l*, no *QQ*	0.145	0.087	1.667	···	···	···
0.0347	11.517	*s*, *QQ*	0.065	0.040	1.625	···	···	···
0.0347	11.517	*m*, *QQ*	0.095	0.056	1.696	···	···	···
0.0347	11.517	*l*, *QQ*	1.140	0.450	2.533	0.86	0.69	1.25
0.1381	11.517	*s*, no *QQ*	0.068	0.041	1.659	···	···	···
0.1381	11.517	*m*, no *QQ*	0.115	0.064	1.797	···	···	···
0.1381	11.517	*l*, no *QQ*	0.174	0.096	1.813	···	···	···
0.1381	11.517	*s*, *QQ*	0.073	0.056	1.304	···	···	···
0.1381	11.517	*m*, *QQ*	0.124	0.067	1.851	5.54	3.11	1.78
0.1381	11.517	*l*, *QQ*	1.330	0.388	3.428	0.33	0.33	1.00
0.348	11.517	*s*, no *QQ*	0.092	0.046	2.000	6.78	4.68	1.45
0.348	11.517	*m*, no *QQ*	0.250	0.093	2.688	2.16	1.74	1.24
0.348	11.517	*l*, no *QQ*	0.827	0.272	3.040	0.60	0.57	1.05
0.348	11.517	*s*, *QQ*	0.094	0.047	2.000	6.80	···	···
0.348	11.517	*m*, *QQ*	0.294	0.105	2.800	1.82	1.35	1.35
0.348	11.517	*l*, *QQ*	9.240	2.780	3.324	0.046	0.044	1.05
0.348	7.586	*s*, no *QQ*	0.145	0.062	2.339	3.48	3.72	0.94
0.348	7.586	*m*, no *QQ*	0.334	0.122	2.738	1.56	1.50	1.04
0.348	7.586	*l*, no *QQ*	1.444	0.452	3.195	0.33	0.30	1.10
0.348	7.586	*s*, *QQ*	0.145	0.063	2.302	4.63	3.08	1.50
0.348	7.586	*m*, *QQ*	0.530	0.180	2.944	0.84	0.97	0.87
0.348	7.586	*l*, *QQ*	>13	10.400	···	0.026	0.023	1.13

[a] $\tau(\text{ps}) = 3.762\,\tau^*$.

[b] Calculated from the condition $\ln\langle P_j[\cos\theta(\tau_j)]\rangle = -1$ ($j = 1,2$; $P_j = j$th Legendre polynomial).

[c] $D_R(\text{ps}^{-1}) = 2.658\times10^{-1}\,D_R^*$

[d] Calculated from the short time limit of the $-\ln\langle P_j[\cos\theta]\rangle$ vs t curve; $\lambda_j D_{Rj} = (d/dt)\{-\ln\langle P_j[\cos\theta(t)]\rangle\}$ ($\lambda_1 = 2$; $\lambda_2 = 6$).

[e] Only values for which the correlation coefficient exceeds 0.96 are reported.

Legendre polynomials can develop plateaus.[18] For nondilute solutions of rod-like polymers, these plateaus have been explained (in terms of Doi–Edwards theory) as a consequence of caging effects imposed on rods by their neighbors.[18] In the present case, the appearance of plateaus or the loss of linearity, both of which we observed in several simulations, indicate that the assumption of uncorrelated motion breaks down at long times. In this sense, the calculation of rotational diffusivities is fundamentally different from that of their translational counterparts, and Eqs. (10) and (11) are not valid at arbitrarily long times.[19] The rotational diffusion coefficients reported here have been calculated, in all cases, over times which are long compared to the initial nonexponential decay, but short with respect to loss of linearity, when this was observed.

The first rotational relaxation time (τ_1^*) is plotted in Fig. 6. The growth in relaxation time with density is evidence of increased hindrance to molecules' ability to rotate freely. This effect is more pronounced the higher the elongation and quadrupole moment. This behavior is in contrast with translational relaxation, the characteristic time for which always decreases with density as long as the system retains its fluid character. Trends for τ_2^* are similar in all cases (see Table IV).

If we select a ratio of relaxation times within 20% of the theoretical value (i.e., $2.4 < \tau_1^*/\tau_2^* < 3.6$) as a criterion of compliance with Debye-type behavior, several trends emerge from the data in Table IV. At low and intermediate densities, only the long molecule with quadrupolar interactions included exhibits Debye-type behavior. At liquid-like densities ($\rho^* = 0.348$), we observe breakdown of Debye behavior only for the short molecule, irrespective of the presence of quadrupolar interactions.

The calculated relaxation times and diffusion coefficients are trivially related to each other [i.e., via Eqs. (7) and (8)] only if the Debye theory is valid, since the former were calculated by measuring the time it takes for the logarithm of a Legendre polynomial to decay to a fixed value, and the latter, from the slope of the time dependence of the logarithm of the corresponding Legendre polynomial. The time-dependent behavior of the two first Legendre polynomials is shown in Fig. 7. Figure 7(a) illustrates the evolution of $\langle P_1(\cos\theta)\rangle$ at liquid-like density ($T^* = 11.517$), and Fig. 7(b), the evolution of $\langle P_2(\cos\theta)\rangle$ at the intermediate density.

Figure 8 shows the time dependence of $\langle\theta^2\rangle$ for the three quadrupolar systems. Note that $\theta(t)$ is the instantaneous angle between orientations separated by a time t; according-

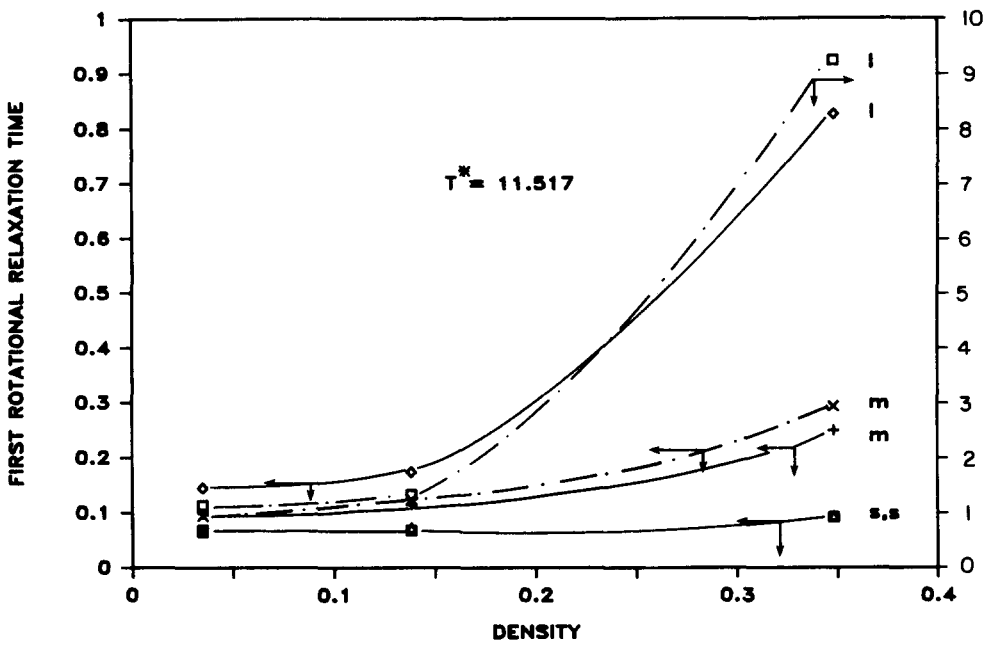

FIG. 6. Dependence of the first rotational relaxation time (τ_1^*) upon density (ρ^*) for nonquadrupolar (—) and quadrupolar (–·–) systems. $T^* = 11.517$. *s*, *m*, and *l* denote the small, medium, and long molecule, respectively. τ_1 is obtained from the condition $\ln\langle P_1(\cos\theta)\rangle = -1$.

ly, $\langle\theta^2\rangle$ does not grow without limits[17,18] and should not be confused with the mean squared angular displacement with respect to a fixed orientation.[16–18] As with the Legendre polynomials, ensemble averages were computed by averaging over molecules and initial times. At low and intermediate densities the theoretically predicted limit $[\langle\theta^2\rangle \to (\pi^2 - 4)/2 = 2.93$, see Eq. (5)] is attained in all cases. The slower relaxation of the long molecule [Fig. 8(a)] is indicative of the importance of quadrupole-induced angular correlations at low density.

At the lowest, gas-like density [$\rho^* = 0.0347$; Fig. 8(a)], both the short and medium molecules overshoot the long-time $\langle\theta^2\rangle$ limit. Since $\langle\theta\rangle = \pi/2$ indicates uncorrelated orientations, this short-time overshoot is tantamount to a negative correlation with respect to an initial configuration. Analogous behavior, in the case of velocity autocorrelation functions, is known to be hydrodynamic in nature.[20] The behavior shown in Fig. 8(a), however, is not hydrodynamic: it disappears upon increasing density, and occurs because both the short and medium molecules experience large angular displacements between "collisions." From Fig. 8(a), and using $\langle\theta^2\rangle^{1/2} \sim \langle\theta\rangle$ for estimating purposes, it follows that a short molecule experiences, on average, an angular displacement of 0.7π (peak of $\langle\theta^2\rangle \sim 4.87$) before undergoing appreciable interactions.

Also shown in Fig. 8(b) are theoretical predictions of $\langle\theta^2(t)\rangle$ according to Eq. (5), for the long molecule (this calculation is only meaningful when there is close agreement between D_{R1} and D_{R2}; see Table IV). Equation (5) is valid for long times. In particular, the condition[17] $t^* \gg (10D_R^*)^{-1}$ implies $t^* \gg 0.3$ ($\rho^* = 0.1381$), $t^* \gg 2.3$ ($\rho^* = 0.348$, $T^* = 11.517$), and $t^* \gg 4.2$ ($\rho^* = 0.348$, $T^* = 7.586$). At medium density, when the long-time condition can easily be satisifed within the time span of a simulation, there is good agreement with the Debye-based calculations: for $t^* = 2,4,6,8$, and 10, the mean squared angles equal {2.04 (simulation), 1.97 [Eq. (5)]}, (2.62, 2.67), (2.83, 2.86), (2.87, 2.91), and (2.80, 2.93), respectively.

The importance of electrostatic interactions in slowing down rotational dynamics can be seen by comparing rotational relaxation times for the long molecule, with and without quadrupole (Table IV): $\tau_1(\text{QQ})/\tau_1$ (no QQ) equals 7.86 at low density, 7.64 at medium density, and 11.17 at liquid-like density ($T^* = 11.517$). The strong orientational correlations imposed by quadrupolar interactions are absent in the purely Lennard-Jones case.

Further evidence of hindered rotation at liquid-like density was also found by Steele and Streett[5] in their study of diatomic Lennard-Jonesiums with quadrupolar interactions. These authors studied short molecules (elongation = 0.592 in our units), at $\rho^* = 0.413$ and $T^* = 6.304$, and suggested the appropriateness of a libration-based model to describe rotational dynamics in orientationally correlated fluids.

The short-time behavior of $\langle\theta^2(t)\rangle$ is directly related to infrared or Raman measurements of $\langle\cos\theta(t)\rangle$ on the picosecond time scale,[21] since $\langle\theta^2(t)\rangle \approx 2(1 - \langle\cos\theta(t)\rangle)$ for $\langle\theta^2(t)\rangle \ll 12$. Numerous examples of such measurements for simple molecules such as carbon monoxide, carbon tetrachloride, or chloroform are available.[21] For long times, low frequency electric birefringence measurements of rotational relaxation kinetics[22] provide an independent estimate of $\langle\theta^2(t)\rangle$ in cases where this quantity exhibits plateau-type behavior [Fig. 8(b); curve *l*]. In this approach, which is based on Doi and Edwards' theory,[23] $\langle\theta^2(t)\rangle^{0.5}$ is the average angle spanned by the linear molecule confined in a cage during the cage's lifetime.

Viscosity

Shear viscosity coefficients were calculated from the expression[24]

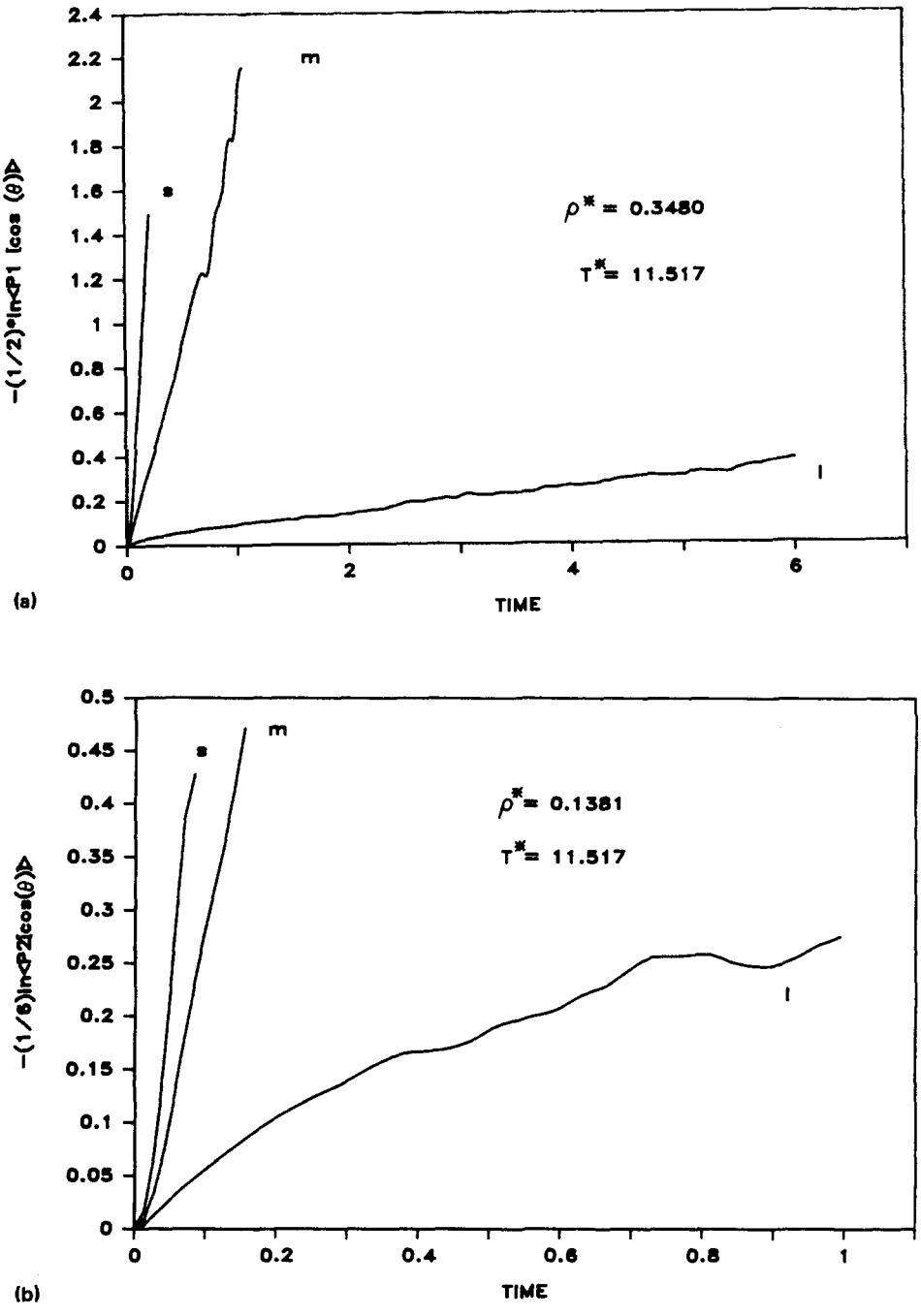

FIG. 7. (a) Evolution of the first rotational Legendre polynomial for a system composed of quadrupolar molecules, at $\rho^* = 0.3480$ and $T^* = 11.517$. (b) Evolution of the second rotational Legendre polynomial for a system composed of quadrupolar molecules, at $\rho^* = 0.1381$ and $T^* = 11.517$. *s*, *m*, and *l* denote the small, medium, and long molecule, respectively. Time is in units of $\sigma_{CC}\sqrt{m_{CO_2}/\epsilon_{CC}}$.

$$\eta = \frac{1}{2VkT}\left\langle \frac{d}{dt}\sum_{j=1}^{N}\left[r_{ij}(t)p_{kj}(t) - r_{ij}(0)p_{kj}(0)\right]^2 \right\rangle, \tag{12}$$

where the time derivative is taken in the long time limit, and where $r_{ij}p_{kj}$ is the product of the ith component of particle j's center-of-mass coordinates and the k th component of particle j's linear momentum ($i \neq k$). Ensemble averaging, in this case, is over initial times, and over the six possible combinations of $r_{ij}p_{kj}$ with $i \neq k$ (i.e., xy, xz, yz and their symmetric counterparts). No statistically significant difference was found between η calculated via Eq. (12) (with due allowance for the system's periodicity) and the same quantity computed from Hoheisel and Vogelsang's stress tensor-explicit version.[25] In the present case, the "displacement" in Eq. (12) was calculated as

$$\begin{aligned} &r_{ij}(t)p_{kj}(t) - r_{ij}(0)p_{kj}(0) \\ &\quad = \Sigma_{n=1}^{t/\Delta t}\{r_{ij}(n\Delta t)p_{kj}(n\Delta t) \\ &\qquad - r_{ij}[(n-1)\Delta t\,]p_{kj}[(n-1)\Delta t\,]\}. \end{aligned} \tag{13}$$

Incremental "displacements" were computed taking into consideration the system's periodic boundary conditions. The correlation coefficient for the linear regression of the slope involved in the calculation of η via Eq. (12) was greater than 0.99 in all cases reported here.

Calculated shear viscosities are listed in Table III. In all cases the value of this property increases with density for a

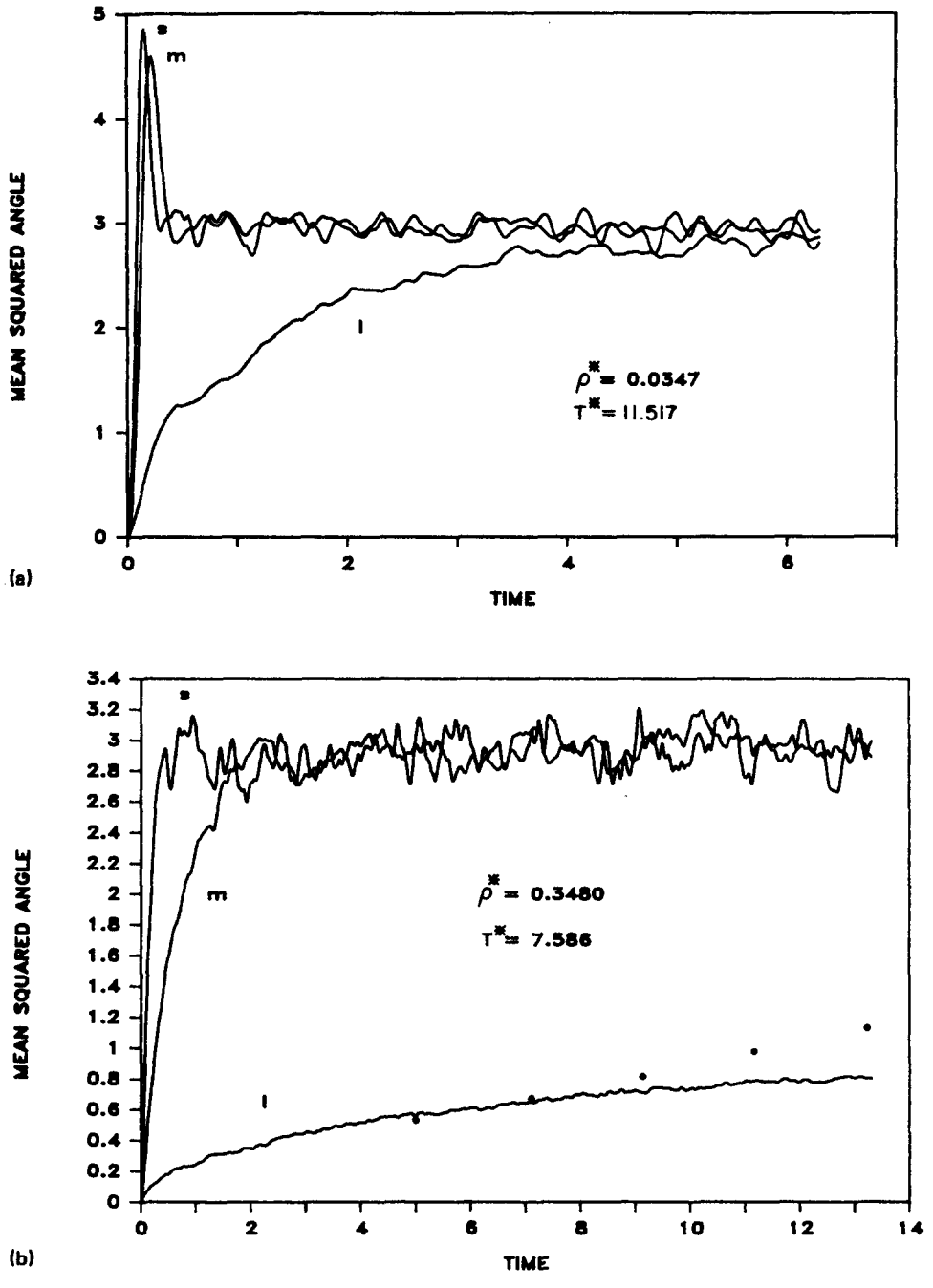

FIG. 8. Evolution of the mean squared angles between orientations ($\langle\theta^2\rangle$) for quadrupolar systems. Conditions are as follows: (a) $[\rho^* = 0.0347, T^* = 11.517]$; (b) $[\rho^* = 0.348, T^* = 7.586]$. s, m, and l denote the small, medium, and long molecule, respectively. Time is in units of $\sigma_{CC}\sqrt{m_{CO_2}/\epsilon_{CC}}$ Points are theoretical calculations, as per Eq. (5).

given elongation and quadrupole (including zero quadrupole). At constant density and elongation, introduction of a quadrupole moment results in a viscosity decrease. No clear trend emerges from Table III for the elongation dependence of viscosity at constant number density. Viscosity changes are within the statistical uncertainty of $\pm$ 13% (see the Appendix), with the exception of the long molecule at low density. In this case, the viscosity is significantly higher (lower) than that for the short and medium molecules in the absence (presence) of quadrupolar interaction.

This relative insensitivity of viscosity to elongation changes could in principle be explained in terms of a rough balance between packing and orientational effects, but further research is needed here. A detailed investigation of the importance of orientational order with respect to momentum transfer in linear molecular fluids is currently in progress. This study is especially significant in the light of the pronounced reductions in viscosity which resulted, in every case, upon addition of a quadrupole moment.

The calculation of shear viscosities via Eq. (12) involves only an average over initial times, whereas diffusivity calculations involve averaging over initial times and over all molecules. There being no other way of ascertaining the statistical significance of viscosity calculations, except for performing averages over several runs (see the Appendix), or by comparing with nonequilibrium[26] simulation results, we merely point out here the need for comparative studies of viscosity calculations for molecular fluids using different techniques.

CONCLUSION

Quadrupolar interactions give rise to behavior which differs in important ways from that exhibited by otherwise identical but quadrupole-free systems. Whereas the configurational energy decreases in magnitude as the molecular elongation is increased isochorically and isothermally in a system composed of nonquadrupolar linear molecules, it increases in magnitude when the same perturbation is introduced in a quadrupolar system with given partial site charges. Similarly, pressure is a monotonically increasing function of elongation at constant density and temperature in the absence of quadrupolar interactions, but shows a maximum at intermediate elongations for quadrupolar systems. The latter phenomenon is a consequence of the fact that increasing the elongation at constant quadrupole and increasing the quadrupole at constant elongation have opposite effects on the pressure, the former perturbation tending to increase it, and the latter to decrease it.

Center-of-mass mobility is invariably reduced by the presence of quadrupolar interactions vis-a-vis a system composed of nonquadrupolar linear molecules of identical elongations. Furthermore, rotational relaxation tends to be considerably slower in the presence of quadrupolar interactions. This suggests the presence of orientational correlations in dense systems whose constituent molecules have a strong quadrupole moment. Work on this topic is currently in progress.

Quadrupole-induced hindered rotational mobility leads to smaller angular displacements per unit time and, consequently, to Debye-type behavior under density and temperature conditions at which quadrupole-free systems do not exhibit exponentially decaying rotational Legendre polynomials.

ACKNOWLEDGMENTS

The authors gratefully acknowledge the financial support of the U.S. Department of Energy, Office of Basic Energy Sciences, Division of Chemical Sciences (Grant No. DE-FG02-87ER13714). Calculations were performed on a Cyber 205 machine located at the John von Neumann National Supercomputer Center, Princeton, NJ, and on a Cyber 205 machine located at the Florida State University Supercomputer Computations Research Institute, which is partially funded by the U.S. Department of Energy, through Contract No. DE-FG02-85ER2500.

APPENDIX

All simulations were performed at constant number of particles, volume, and temperature (N,V,T). Site–site interactions were treated as shifted-force[27] Lennard-Jonesiums, with parameters as per Table I, and truncation at 8.438 Å (i.e., 3.03 σ_{cc}). Quadrupolar interactions were treated via a central potential[13]

$$\phi_{ij} = \frac{3Q_i'Q_j'}{4r_{ij}^5}\{1 - 5(\hat{\mathbf{r}}_{ij}\cdot\hat{\mathbf{l}}_i)^2 - 5(\hat{\mathbf{r}}_{ij}\cdot\hat{\mathbf{l}}_j)^2 - 15(\hat{\mathbf{r}}_{ij}\cdot\hat{\mathbf{l}}_i)^2(\hat{\mathbf{r}}_{ij}\cdot\hat{\mathbf{l}}_j)^2 + 2[\hat{\mathbf{l}}_i\cdot\hat{\mathbf{l}}_j - 5(\hat{\mathbf{r}}_{ij}\cdot\hat{\mathbf{l}}_i)(\hat{\mathbf{r}}_{ij}\cdot\hat{\mathbf{l}}_j)]^2\}, \quad \text{(A1)}$$

where $(4\pi\epsilon_0)^{1/2}Q'$ is the quadrupole moment on the ith molecule, ϵ_0 is the permittivity of free space (see Table I), r_{ij} is the center-of-mass distance between molecules i and j, $\hat{\mathbf{r}}_{ij}$, a unit vector pointing from the center-of-mass of j to the center of mass of i, and $\hat{\mathbf{l}}_i$ is the unit orientation vector coaxial with molecule i. Quadrupolar interactions were truncated at 8.438 Å.

In order to ascertain the reproducibilty of the calculated properties, a 10 000 step simulation for the medium molecule, with quadrupolar interactions was performed $(m,\mathrm{QQ},\rho^* = 0.1381, T^* = 11.517, N = 256)$. The calculated energy (U^*) and the pressure (P^*) were -17.31 and 1.15. Comparison with the production run reported in Table III ($U^* = -17.51, P^* = 1.14$) indicates changes of 1.14% (U^*) and 0.9% (P^*). The calculated translational diffusion coefficient (D_t^*) and shear viscosity (η^*) in the control run were 2.56 and 1.7, whereas the values obtained in the production run (Table III) were 2.43 (D_t^*) and 1.6 (η^*), indicating changes of 5.3% (D_t^*) and 6.3% (η^*). Note that, for transport properties, statistical errors can only be determined by averaging over several simulations.[28]

In simulations including quadrupolar interactions, the translational equations of motion were integrated with a fifth-order predictor-corrector algorithm,[29] whereas the rotational equations were integrated via a fourth-order predictor-corrector scheme. Rotational kinematics was described via quaternions,[30] using the singularity-free approach due to Evans and Murad.[31] Thermostating was implemented by applying separate momentum scaling to the translational and rotational motion.[32] A center-of-mass Verlet neighbor list approach[33] was used in order to compute pair interactions efficiently, with neighbor list cutoff at 9.274 Å $+ 2d_{CO}$ (10.388 Å $+ 2d_{CO}$ for low density simulations), and updating every ten steps,[34] where $2d_{CO}$ is the oxygen–oxygen separation.

In order to ascertain the influence of momentum scaling upon the calculated transport properties, a 10 000 step constant energy (N,V,E) simulation was performed, for the medium molecule, with quadrupolar interactions $(m,\mathrm{QQ},\rho^* = 0.1381, N = 256)$. The average temperature $\langle T^* \rangle$ was 11.678 [1.4% higher than in the production and (N,V,T) test run mentioned above]. The calculated translational diffusion coefficient and shear viscosity were 2.39 (D_t^*) and 1.8 (η^*). Comparison with production run values of 2.43 (D_t^*) and 1.6 (η^*; Table III) indicates changes of 1.65% in translational diffusion and 12.5% in viscosity due to momentum scaling (note, however, that the temperatures, as mentioned above, were not identical). The corresponding (N,V,E) thermodynamic quantities were -17.56 (U^*) and 1.21 (P^*), which differ by 0.3% and 6.1%, respectively, from the production run values at $T^* = 11.517$ (Table III). Energy conservation in the (N,V,E) run was 0.0085

parts in 10^4 per time step, indicating negligible influence of quadrupole truncation.

Based on the above mentioned tests on reproducibility and on the effects of momentum scaling, as well as on several subsequent test runs at different state conditions, we adopted conservative values of $\pm 6\%$ and $\pm 13\%$ for the statistical uncertainties associated with the reported values of D_t^* and η^*, respectively. As a comparison, we cite the work of Levesque and Verlet,[28] who conclude that, for atomic systems, statistical uncertainties of $\sim 4\%$ in shear viscosity can be obtained only if simulations as long as 1000 ps are performed (266 in our time units).

In the absence of quadrupolar interactions, both rotational and translational equations were integrated via a Verlet scheme,[33] with rotational kinematics as described above. Thermostating was implemented by applying Gauss' Principle of Least Constraints.[35–37] In order to compute pair interactions efficiently, a modified version of the recently proposed Brode–Ahlrichs diagonal scheme[38] was used, the modification consisting of calculating the distance matrix for all pairs of sites, and eliminating intramolecular interactions before calculating the forces.

System sizes for all of the simulations performed in this work are shown in Table V. The integration step for the simulations including quadrupolar interactions was $7\times10^{-4}\,\sigma_{CC}\sqrt{m_{CO_2}/\epsilon_{CC}}$, and $3.335\times10^{-4}\,\sigma_{CC}\sqrt{m_{CO_2}/\epsilon_{CC}}$ for nonquadrupolar studies. In order to verify the insensitivity of calculated properties to changes in the numerical scheme (i.e., Verlet vs predictor-corrector, Brode–Ahlrichs vs neighbor list), two test runs were performed on the medium molecule ($T^* = 11.517$, $\rho^* = 0.348$), in the absence of quadrupolar interactions, and using the two different simulation methodologies. Equilibrium properties differed by less than 1%. The calculated translational diffusion coefficient (D_t^*), first, and second rotational relaxation times (τ_1^*, τ_2^*) were 2.47, 0.113, and 0.100, respectively (predictor-corrector, neighbor list algorithm), and 2.54, 0.115, and 0.064 (Verlet, Brode–Ahlrichs algorithm). Note that, whereas pressure, energy, and translational diffusivity are true properties, the rotational relaxation times are qualitative measures of rotational dynamics and become properties only in the Debye limit, when the Legendre polynomials decay exponentially.

TABLE V. System sizes for the simulations performed in this work.

ρ^* $(\rho\sigma_{CC}^3)$	T^* (kT/ϵ_{CC})	System	N
0.0347	11.517	*s*, no *QQ*	125
0.0347	11.517	*m*, no *QQ*	125
0.0347	11.517	*l*, no *QQ*	125
0.0347	11.517	*s*, *QQ*	500
0.0347	11.517	*m*, *QQ*	500
0.0347	11.517	*l*, *QQ*	500
0.1381	11.517	*s*, no *QQ*	125
0.1381	11.517	*m*, no *QQ*	125
0.1381	11.517	*l*, no *QQ*	216
0.1381	11.517	*s*, *QQ*	256
0.1381	11.517	*m*, *QQ*	256
0.1381	11.517	*l*, *QQ*	256
0.348	11.517	*s*, no *QQ*	216
0.348	11.517	*m*, no *QQ*	243
0.348	11.517	*l*, no *QQ*	512
0.348	11.517	*s*, *QQ*	256
0.348	11.517	*m*, *QQ*	500
0.348	11.517	*l*, *QQ*	500
0.348	7.586	*s*, no *QQ*	216
0.348	7.586	*m*, no *QQ*	343
0.348	7.586	*l*, no *QQ*	512
0.348	7.586	*s*, *QQ*	256
0.348	7.586	*m*, *QQ*	500
0.348	7.586	*l*, *QQ*	500

An accurate comparison between the pressure and energy calculated for the base quadrupolar case (*m*,QQ) and analogous computations by Murthy *et al.* (model C)[4] is not possible, since these authors do not report their cutoff distance for force and potential evaluations. Nevertheless, we performed a test simulation using truncation at 8.91 Å, at identical conditions as those used by Murthy *et al.*[4] ($\rho^* = 0.346$, $T^* = 7.6$), and obtained $U^* = -59.2$, $P^* = -0.970$, where Murthy *et al.*[4] obtained $U^* = -58.08$, $P^* = -0.485$.

Initial center-of-mass positions corresponded to an fcc lattice (quadrupolar simulations), and to a simple cubic lattice for nonquadrupolar studies. Orientations corresponding to an α-fcc structure were initially assigned to the quadrupolar systems; the nonquadrupolar simulations were started from either random ($\rho^* = 0.0347, \rho^* = 0.1381$) or ordered $[\hat{\mathbf{l}} = (\sqrt{3}/3)\hat{\mathbf{i}} + (\sqrt{3}/3)\hat{\mathbf{j}} + (\sqrt{3}/3)\hat{\mathbf{k}}; \rho^* = 0.348]$ orientational configurations. Random translational and rotational velocity components corresponding to the desired temperature were assigned, and the ordered structure was allowed to melt for a number of steps which varied from 3000 to 20 000 time steps. Simulations were always at least 20 000 time steps (i.e., approximately 53 ps for quadrupolar studies, and 25 ps for the nonquadrupolar studies).

Time averages were computed by performing several "experiments" with displaced origin in the course of a given simulation. In the quadrupolar studies, ten such experiments were conducted, each separated by ten time steps,[39] and lasting 19 900 time steps. In the nonquadrupolar studies, ten experiments were conducted, separated by 1000 time steps, and each lasting 11 000 time steps.

We now discuss the calculated properties for the CO_2-like system (*m*,QQ; see Table I). Simulated and experimental data are compared in Table VI. The shifted-force[27] RTSLJQ with parameters as per Table I overpredicts pressures. Agreement at the subcritical density ($\rho^* = 0.0347$; $\rho = 2668$ mol/m^3), though, is good. This, of course, would call for a detailed tuning of potential parameters if the shifted-force RTSLJQ were used as a predictive model for CO_2; as has already been stated, however, this is not the goal of this work.

Shear viscosities are substantially higher than experimental values (see Table VI). It is not at present possible to ascertain whether this discrepancy is a consequence of the nonpredictive nature of the potential, or if it reflects inherent

TABLE VI. Calculated and experimental properties for the CO_2-like system (m, QQ).

T (K)	ρ (mol/m^3)	P^a (bar)	η^a (cp)	D_t [a] (cm^2/s)	P^b (bar)	η^b (cp)
334	2668	65.3	0.0693	2.04×10^{-3}	58	0.0188
334	10620	211.4	0.1140	5.00×10^{-4}	128	0.0383
334	26721	2427	0.3220	7.9×10^{-5}	...	...
220	26721	514	...	...	60	...

[a] Calculated via MD (see Table III). Blank values were not calculated in this work.

[b] Experimental (Ref. 40). Blank values either not available experimentally or not calculated in this work.

limitations in the statistical significance of computations according to Eq. (12) with sample sizes of order 10^2 and run durations of order 10^4 time steps.

As for translational diffusion coefficients, we note in the first place the constancy of ρD_t up to the critical density, in agreement with elementary kinetic theory. The magnitude of D_t is also in qualitative agreement with the measurements of Robb and Drickamer[41] at slightly different conditions: at 315 K, these investigators obtained $D_t = 4.88\times10^{-4}$ cm^2/s ($\rho = 9091$ mol/m^3), $D_t = 3.43\times10^{-4}$ cm^2/s ($\rho = 11364$ mol/m^3), and $D_t = 2.87\times10^{-4}$ cm^2/s ($\rho = 13636$ mol/m^3).

[1] D. Brown and J. H. R. Clarke, J. Chem. Phys. **86**, 6446 (1987).
[2] C. Hoheisel, J. Chem. Phys. **89**, 7457 (1988).
[3] A. D. Buckingham and R. L. Disch, Proc. R. Soc. London Ser. A **273**, 275 (1963).
[4] C. S. Murthy, K. Singer, and I. R. McDonald, Mol. Phys. **44**, 135 (1981).
[5] W. A. Steele and W. B. Streett, Mol. Phys. **39**, 279 (1980).
[6] K. Singer, J. V. L. Singer, and A. J. Taylor, Mol. Phys. **37**, 1239 (1979).
[7] V. N. Kabadi and W. A. Steele, J. Phys. Chem. **89**, 1467 (1985).
[8] S. S. Wang, C. G. Gray, P. A. Egelstaff, and K. E. Gubbins, Chem. Phys. Lett. **21**, 123 (1973).
[9] K. S. Shing and K. E. Gubbins, Mol. Phys. **45**, 129 (1982).
[10] K. S. Shing, J. Chem. Phys. **85**, 4633 (1986).
[11] M. R. Stapleton, D. J. Tildesley, N. Quirke, and A. Z. Panagiotopoulous, Mol. Simul. **2**, 147 (1989).
[12] C. A. English and J. A. Venables, Proc. R. Soc. London Ser. A **340**, 57 (1974).
[13] C. G. Gray and K. E. Gubbins, *Theory of Molecular Fluids* (Clarendon, Oxford, 1984), p. 83.
[14] R. C. Reid, J. M. Prasunitz, and B. E. Poling, *The Properties of Gases and Liquids*, 4th ed. (McGraw-Hill, New York, 1987), p. 667.
[15] W. B. Streett and D. J. Tildesley, Proc. R. Soc. London Ser. A **355**, 239 (1977).
[16] P. Debye, *Polar Molecules* (Dover, New York, 1929), Chap. V.
[17] J. J. Magda, H. T. Davis, and M. Tirrell, J. Chem. Phys. **85**, 6674 (1986).
[18] I. Bitsanis, H. T. Davis, and M. Tirrell, *Macromolecules* **21**, 2824 (1988).
[19] J. P. Hansen and I. R. McDonald, *Theory of Simple Liquids* 2nd ed. (Academic, London, 1986), Sec. 12.12, p. 501.
[20] L. E. Reichl *A Modern Course in Statistical Physics* (University of Texas, Austin, 1980), Chap. 16.
[21] W. G. Rothschild, *Dynamics of Molecular Liquids* (Wiley, New York, 1984).
[22] Y. Mori, N. Ookubo, R. Hayakawa, and Y. Wada, J. Polym. Sci. **20**, 211 (1982).
[23] M. Doi and S. F. Edwards, *Theory of Polymer Dynamics* (Clarendon, Oxford, 1986).
[24] D. A. McQuarrie, *Statistical Mechanics* (Harper and Row, New York, 1976), p. 519.
[25] C. Hoheisel and R. Vogelsang, Comp. Phys. Rep. **8**, 1 (1988).
[26] P. T. Cummings and T. L. Varner, J. Chem. Phys. **89**, 6391 (1988).
[27] W. B. Streett, D. J. Tildesley, and G. Saville, in *Computer Modelling of Matter*, edited by P. Lykos, ACS Symp. Ser. 86 (Americal Chemical Society, Washington, DC, 1978), Chap. 13.
[28] D. Levesque and L. Verlet, Mol. Phys. **61**, 143 (1987).
[29] C. W. Gear, *Numerical Initial Value Problems in Ordinary Differential Equations* (Prentice-Hall, Englewood Cliffs, 1971).
[30] H. Goldstein, *Classical Mechanics*, 2nd ed. (Addison-Wesley, Reading, MA, 1980), Chap. 4.
[31] D. J. Evans and S. Murad, Mol. Phys. **34**, 327 (1977).
[32] J. M. Haile and S. Gupta, J. Chem. Phys. **79**, 3067 (1983).
[33] L. Verlet, Phys. Rev. **159**, 98 (1967).
[34] A. A. Chialvo and P. G. Debenedetti, *Proceedings of the Fourth International Conference on Supercomputing*, Santa Clara, **II**, 117 (1989).
[35] K. F. Gauss, J. Reine Angew. Math., **iv**, 232 (1829).
[36] A. D. Simmons, and P. T. Cummings, Chem. Phys. Lett. **129**, 92 (1986).
[37] D. J. Evans, W. G. Hoover, B. H. Failor, B. Moran, and A. J. C. Ladd, Phys. Rev. A **28**, 1016 (1983).
[38] S. Brode and R. Ahlrichs, Comp. Phys. Commun. **42**, 51 (1986).
[39] M. P. Allen and D. J. Tildesley *Computer Simulation of Liquids* (Clarendon, Oxford, 1987), p. 187.
[40] N. B. Vargaftik, *Handbook of Physical Properties of Liquids and Gases. Pure Substances and Mixtures*, 2nd ed. (Hemisphere, Washington, 1975), Chap. 3.
[41] W. L. Robb and H. G. Drickamer, J. Chem. Phys. **19**, 1504 (1951).